European Journal of Pharmacology 911 (2021) 174525

Contents lists available at ScienceDirect

European Journal of Pharmacology

journal homepage: www.elsevier.com/locate/ejphar

Stereospecific inhibition of AMPK by (*R*)-crizotinib induced changes to the morphology and properties of cancer and cancer stem cell-like cells

Tae Hyun Kim [a,1], Jong Hyeok Park [a,1], Jooyeon Park [a,1], Dong Min Son [a], Ji-Young Baek [a], Hee Jun Jang [a], Won Ki Jung [a], Youngjoo Byun [a,**], Sang Kyum Kim [b], Song-Kyu Park [a,c,*]

[a] College of Pharmacy, Korea University, Sejong, Republic of Korea
[b] College of Pharmacy, Chungnam National University, Daejeon, Republic of Korea
[c] Research Driven Hospital, Korea University Guro Hospital, Biomedical Research Center, Seoul, Republic of Korea

ARTICLE INFO

Keywords:
Crizotinib
Morphology
AMPK
Cancer
Enantiomer

ABSTRACT

Crizotinib is used in the clinic for treating patients with ALK- or ROS1-positive non-small-cell lung carcinoma. The objective of the present study was to determine if crizotinib enantiomers could induce changes to the properties of cancer and cancer stem cell (CSC)-like cells at a high concentration (~ 3 μM). While (*R*)-crizotinib induced changes in morphologies or sizes of cells, (*S*)-crizotinib did not. Pretreatment with (*R*)-crizotinib suppressed the proliferation of cancer or CSC-like cells *in vitro* and tumor growth *in vivo*. *In vivo* administration of (*R*)-crizotinib inhibited the growth of tumors formed from CSC-like cells by 72%. %. Along with the morphological changes induced by (*R*)-crizotinib, the expression levels of CD44 (NCI-H23 and HCT-15), ALDH1 (NCI-H460), nanog (PC-3), and Oct-4A (CSC-like cells), which appear to be specific marker proteins, were greatly changed, suggesting that changes in cellular properties accompanied the morphological changes in the cells. The expression levels of Snail, Slug, and E-cadherin were also greatly altered by (*R*)-crizotinib. Among several signal transduction molecules examined, AMPK phosphorylation appeared to be selectively inhibited by (*R*)-crizotinib. BML-275 (an AMPK inhibitor) and AMPKα2 siRNA efficiently induced morphological changes to all types of cells examined, suggesting that (*R*)-crizotinib might cause losses of characteristics of cancer or CSCs via inhibition of AMPK. These results indicate that (*R*)-crizotinib might be an effective anticancer agent that can cause alteration in cancer cell properties.

1. Introduction

Although many new therapies have been introduced, cancer is still a leading cause of death. Crizotinib has been developed for treating patients with non-small-cell lung carcinoma (NSCLC). It works by inhibiting anaplastic lymphoma kinase (ALK) (Christensen et al., 2007) and c-ros oncogene 1 (ROS1) (Bergethon et al., 2012). Recently, many clinical studies are being conducted to determine additional activities of crizotinib against various kinds of cancer, including prostate cancer, large cell lung cancer, breast cancer, and neuroblastoma (more information can be obtained from the ClinicalTrial.gov database). Clinical trials for proving its effects in combination with other anticancer agents having different modes of action have also been reported (Patel et al., 2020; Tripathi et al., 2020; Wang et al., 2020).

While the (*R*)-enantiomer of crizotinib is being currently used for patients in the clinic, the (*S*)-enantiomer of crizotinib is not. However, it has been reported that the (*S*)-enantiomer of crizotinib has anticancer activity by inhibiting human MTH1 enzyme that hydrolyzes oxidized purine deoxyribonucleodides (Huber et al., 2014).

Many previous studies have investigated known molecular targets of (*R*)-crizotinib such as ALK and ROS1, but anticancer activities of (*R*)-crizotinib through its off-target effects have also been investigated. Recent studies on its mechanism of action have shown that (*R*)-crizotinib could induce immunogenic cell death (ICD) of cancer (Liu et al., 2019a, 2019b). While (*R*)-crizotinib at submicromolar concentrations is effective against NSCLC cells with a genetic change in the *ALK* gene (Zhang et al., 2011), a high concentration (10 μM) of (*R*)-crizotinib could induce hallmarks of ICD in cancer cell lines (Liu et al., 2019b). In

* Corresponding author. College of Pharmacy, Korea University, 2511 Sejong-ro, Sejong 30019, Republic of Korea.
** Corresponding author.
E-mail addresses: yjbyun1@korea.ac.kr (Y. Byun), spark123@korea.ac.kr (S.-K. Park).
[1] Kim TH, Park JH and Park J contributed equally to this paper.

https://doi.org/10.1016/j.ejphar.2021.174525
Received 17 January 2021; Received in revised form 17 September 2021; Accepted 22 September 2021
Available online 25 September 2021

contrast, (*S*)-crizotinib failed to show such ICD-inducing activity.

Among many tumor therapeutic approaches including anti-angiogenesis, induction of apoptosis, targeting signaling molecules, and inhibition of drug efflux transporters, differentiation induction is a strategy to make cancer cells or cancer stem cells (CSCs) lose their intrinsic properties such as proliferation and self-renewal (Enane et al., 2018). To understand the mechanism of action of crizotinib further, it is necessary to expand study areas for crizotinib to other activities such as differentiation induction that might be caused by off-target effects of (*R*)- or (*S*)-crizotinib.

The effects of (*R*)- or (*S*)-crizotinib enantiomers on cancer cell properties have not been previously studied. In the present study, several cancer cell lines, including lung, colon, and prostate cancer cell lines and a CSC-like cell line, were used to compare the effects of the crizotinib enantiomers on cancer cell properties, such as proliferation, tumorigenicity, and morphology. Results demonstrated that the ability of (*R*)-crizotinib to induce morphological changes to the cancer cell lines was much greater than that of (*S*)-crizotinib. In addition, the tumor-forming ability of cancer or CSC cells was greatly inhibited by (*R*)-crizotinib but not by (*S*)-crizotinib. An important signal transduction event involved in the induction of cancer cell differentiation appeared to be the inhibition of AMPK phosphorylation. These results suggest that (*R*)-crizotinib might be useful in the treatment of solid tumors by altering the properties of cancer cells via AMPK inhibition.

2. Materials and methods

2.1. Reagents and antibodies

(*R*)- crizotinib and *(S)*-crizotinib were purchased from APExBIO (Houston, TX, USA). BML275 and BML257 were purchased from Enzo Life Sciences (Farmingdale, NY, USA). SU11274 and SP600125 were purchased form APExBIO (Houston, TX, USA). Antibody against ALK was purchased from Invitrogen (Carlsbad, CA, USA). Antibodies against β-actin, ALDH1, E-cadherin, Snail, Slug, phospho-ALK, AMPK, phospho-AMPK, Akt, phospho-Akt, CD44, FAK, phospho-FAK, nanog, c-Met, phospho-c-Met, Oct-4A, SAPK/JNK, phospho-SAPK/JNK, mTOR, phospho-mTOR, STAT3, phospho-STAT3, Erk1/2, phospho-Erk1/2, phospho-acetyl-CoA (Ser79), caspase-3, p21 Waf1/Cip, and p27 Kip1 were purchased from Cell Signaling Technology (Danvers, MA, USA). All other reagents were obtained from Sigma Aldrich (St. Louis, MO, USA). Catalog numbers for antibodies can be found in Table S1.

2.2. Cell culture and preparation of PC-3 derived CSC-like cells

Human PC-3 (prostate), LNCaP (prostate), HCT-15 (colon), DLD-1 (colon), NCI-H23 (lung), and NCI-H460 (lung) cancer cells were obtained from American Type Culture Collection (ATCC) (Manassas, VA, USA) and cultured in RPMI 1640 (Corning Inc., Corning, NY, USA) supplemented with 10% fetal bovine serum (Corning Inc., Corning, NY, USA), 100 units/ml penicillin G, and 100 mg/ml streptomycin and incubated at 37 °C in a humidified atmosphere containing 5% CO_2. CSC-like cells were derived from PC-3 cells as described previously (Lee et al., 2019). Briefly, single cells of PC-3 were cultured in serum-free DMEM/F12 medium (R&D systems, Minneapolis, MN, USA) supplemented with 10 ng/ml human recombinant epidermal growth factor (hrEGF, R&D systems, Minneapolis, MN, USA), 10 ng/ml human recombinant basic fibroblast growth factor (hrbFGF, R&D systems, Minneapolis, MN, USA), and 2% B27 supplement. They were cultured in ultra-low attachment culture dishes (100 × 20 mm, Corning Inc., Corning, NY, USA) for 7 days until sufficient amounts of spheroids were formed. Singles cells were prepared from spheroids again. This process was repeated four more times. Singles cells prepared from spheroids were cultured in the above-mentioned serum-free medium using a regular animal cell culture ware. These cells were named PC-3 derived CSC-like cells. CSC-like cells with passage numbers between 2 and 4 were used for experiments.

2.3. Cell growth inhibition assay

Inhibition of cell growth by (*R*)- or (*S*)-crizotinib was determined using sulforhodamine B (SRB) assay as described previously (Skehan et al., 1990). Briefly, cells were seeded into a 96-well plate at a density of 1×10^4 cells/ml to 4×10^4 cells/ml depending on the experiment and incubated at 37 °C in a humidified atmosphere containing 5% CO_2 for 24 h. Cells were treated with crizotinib at 0–10 μM for 48–72 h depending on the experiment, fixed with 50% trichloroacetic acid, and stained with 0.4% SRB in 0.1% acetic acid for 30 min. Excess stain was removed by washing with 1% acetic acid. Stain precipitated in cells was dissolved with 10 mM Tris base (pH 10.5). Absorbance was then measured at 565 nm.

2.4. Staining of cells for observing cell morphology

Cells incubated for 6–7 days in the presence or absence of compounds were fixed with 50% trichloroacetic acid and stained with 0.4% SRB in 0.1% acetic acid. Excess stain was removed by washing with 1% acetic acid. Morphology of cells was observed under an inverted microscope and photographed.

2.5. Determination of cell sizes

Cells were seeded into 60 × 15 mm culture dishes at a density of 8×10^3 cells/ml and incubated at 37 °C in a humidified atmosphere containing 5% CO_2 for 72 h in the presence of (*R*)- or (*S*)-crizotinib at different concentrations (0, 1, or 3 μM). Cells were then trypsinized to prepare single cell suspensions. Suspended cells were placed into slits of a hemocytometer, observed using a microscope, and photographed. Sizes and numbers of cells were determined using ImageJ2 program (NIH, USA).

2.6. Flow cytometry analysis of apoptosis

Single cells were plated at a density of 1×10^5 cells/ml in 60 mm^3 for 24 h and treated with 3 μM of (*R*)- or (*S*)-crizotinib for 24 h. Cells were then collected, washed with ice-cold PBS (pH 7.4) and incubated in the presence of Annexin V and propidium iodide (PI) in the dark for 15 min at room temperature. The samples were analyzed with an LSRFortessa flow cytometer (BD Bioscience, San Jose, CA, USA).

2.7. Western blotting analysis

Protein extracts of cell lysates were resolved on 8–10% sodium dodecyl sulfate (SDS) polyacrylamide gels and transferred to Immobilon-P transfer membranes as described previously (Kang et al., 2012). Transferred membranes were blocked with Tris-buffered saline containing 0.1% Tween-20 (TBST) added with 1% bovine serum albumin and probed with primary antibodies. After washing with TBST, membranes were probed with species-specific horseradish peroxidase (HRP)-conjugated secondary antibodies and developed using an Immobilon western chemiluminescent HRP substrate (Merck Millipore, Burlington, MA, USA).

2.8. In vivo nude mouse xenograft model

Animal study protocol was reviewed and approved by Institutional Animal Care & Use Committee (IACUC) of Korea University, Seoul, Korea (protocol number: KUIACUC-2015-28). Six-week-old female Balb/c nude mice (Charles River Laboratories, Yokohama, Japan) were maintained as previously described (Jung et al., 2017). Cancer cells were suspended in 200 μl of phosphate-buffered saline (pH 7.4) and injected subcutaneously at a concentration of 6×10^6 cells/mouse.

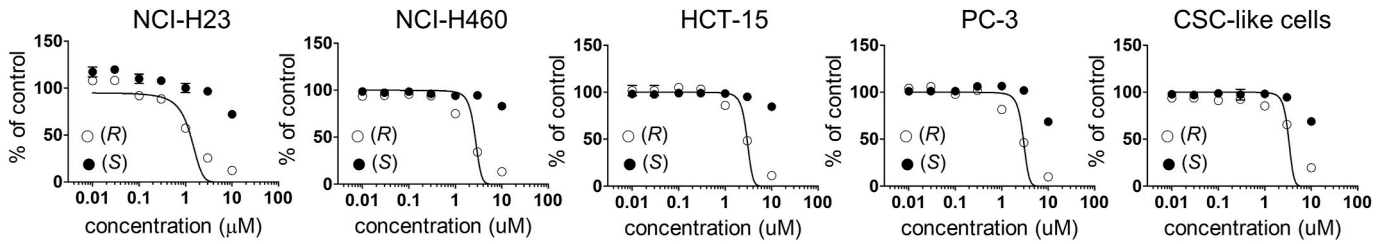

Fig. 1. Growth inhibition of human cancer cells by enantiomers of crizotinib. (A) NCI-H23, NCI-H460, HCT-15, PC-3, and PC-3 derived CSC-like cells were incubated with (*R*)- or (*S*)-crizotinib at various concentrations (0, 0.01, 0.03, 0.1, 0.3, 1, 3, and 10 μM) for 48 h. At the end of the incubation, cells were subjected to sulforhodamine B assay (n = 4) as described in Materials and methods.

Tumor volumes were measured 2 or 3 times a week using a Vernier caliper and calculated using a formula of 0.5 × height × length × width.

2.9. Wound healing assay

Cells were grown to 100% confluency in 24-well plates. Monolayer of cells was then scratched once in the center with a 200 μl pipette tip. Cells were washed with fresh medium, treated with 3 μM of (*R*)- or (*S*)-crizotinib, and allowed to migrate into the wound area at 37 °C in a humidified atmosphere containing 5% CO_2 for 24 h or 36 h. Images were captured using a Nikon TS100-F Inverted Phase Contrast Microscope.

2.10. Measurement of reactive oxygen species (ROS) production by cancer cells

Cells were grown in clear bottom 96-well black plates (Corning, Corning, NY, USA), incubated in the presence or absence of test compound for 48 h at 37 °C, washed with PBS (pH 7.4), and further

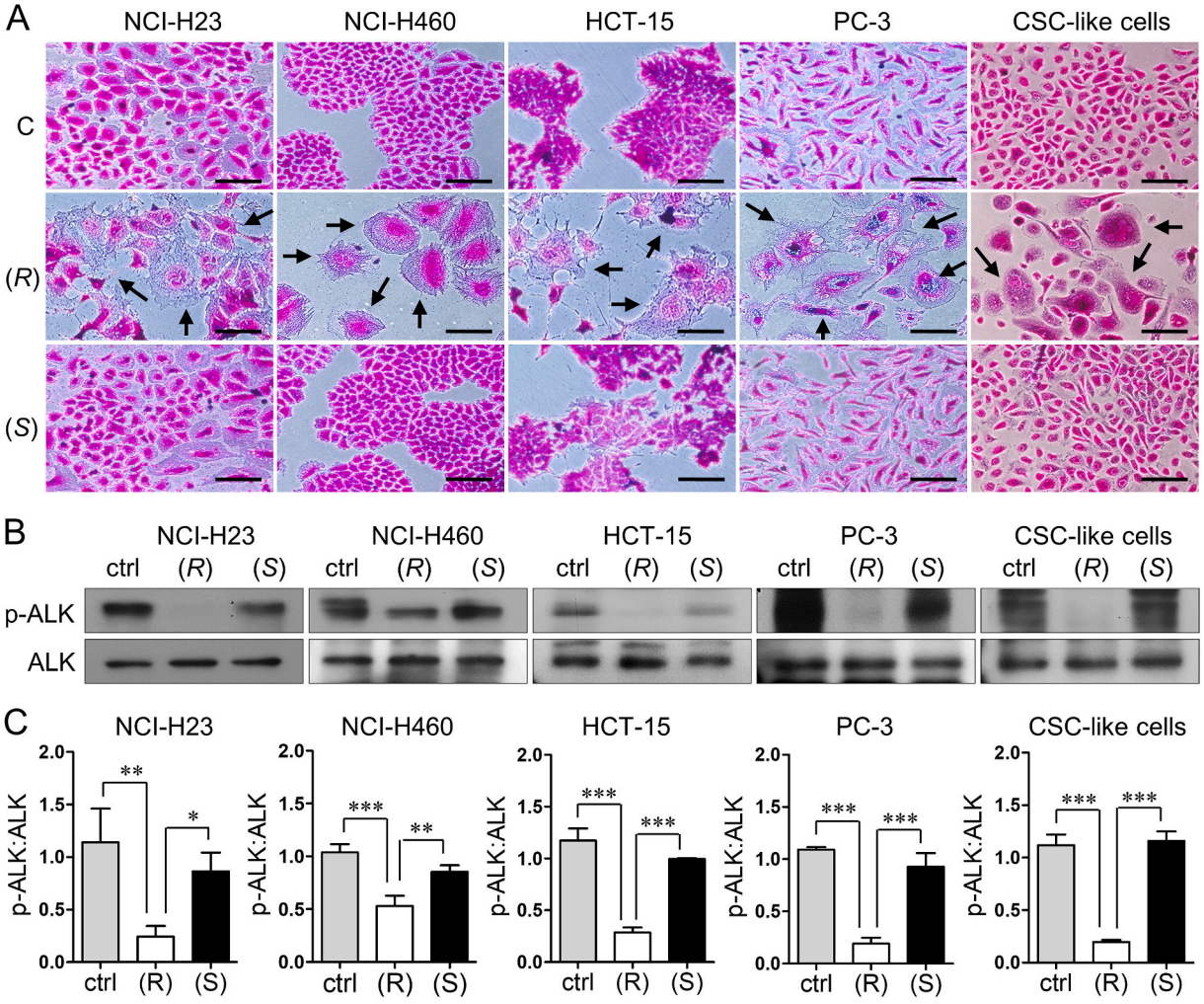

Fig. 2. (*R*)-crizotinib induces morphology changes of human cancer cells and inhibits phosphorylation of ALK. (A) NCI-H23, NCI-H460, HCT-15, PC-3, and PC-3 derived CSC-like cells were incubated with or without 3 μM of (*R*)- or (*S*)-crizotinib for 7 days and then stained with SRB according to the protocol described in Materials and methods. C: control; (*R*): (*R*)-crizotinib; (*S*): (*S*)-crizotinib. Representative images (n = 3) are shown. Black arrows indicate cells whose morphologies are changed. Scale bar: 100 μm. (B) Cells were treated with 3 μM of (*R*)- or (*S*)-crizotinib for 1.5 h, harvested, and subjected to western blotting analysis. (C) Band densities of Western blot images (n = 3) were measured using ImageJ2 program. Data are presented as mean ± SD. *, $p < 0.05$; **, $p < 0.01$; ***, $p < 0.001$. ctrl: control, (R): (*R*)-crizotinib, (S): (*S*)-crizotinib.

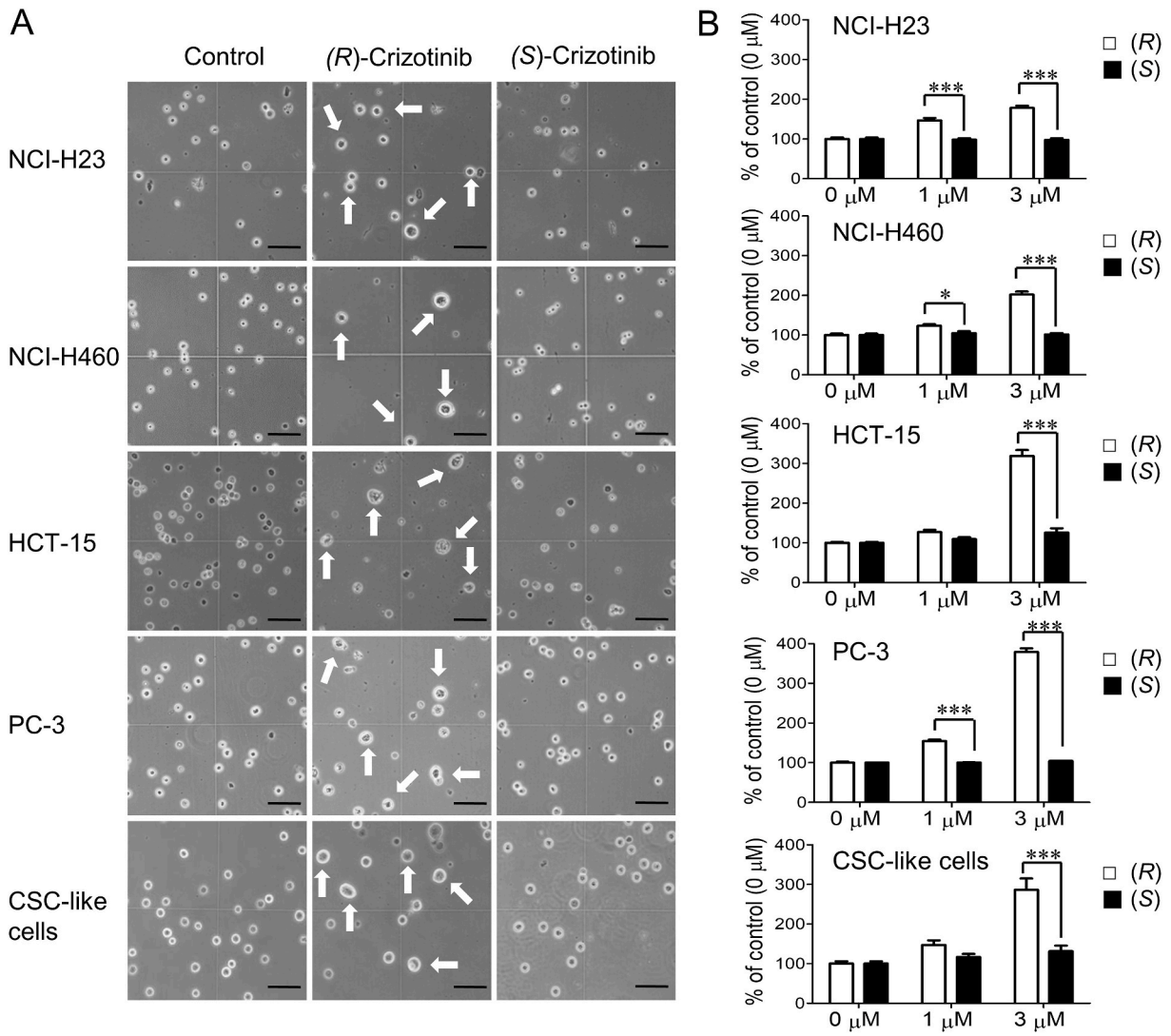

Fig. 3. (*R*)-crizotinib increases sizes of cancer and CSC-like cells. (A) NCI-H23, NCI-H460, HCT-15, PC-3, and PC-3 derived CSC-like cells were incubated with or without 3 μM of (*R*)- or (*S*)-crizotinib for 72 h. They were then trypsinized, suspended in PBS (pH 7.4), and observed under an inverted microscope. White arrows indicate cells increased in sizes. Scale bar: 100 μm. (B) Sizes of cells incubated with (*R*)- or (*S*)-crizotinib at various concentrations (0, 1, and 3 μM) for 72 h were measured (n = 3) using Image J2 program. Data are presented as mean ± SD. **, $p < 0.01$; ***, $p < 0.001$.

incubated in the presence of H2DCFDA (2′,7′-dichlorofluorescin diacetate) for 18 h at 37 °C. At the end of the incubation, cells were washed twice with PBS (pH 7.4). Fluorescence of DCF (2′,7′-dichlorofluorescin) was then read at Excitation/Emission wavelengths of 485/530 nm.

2.11. Transfection of AMPKα2 siRNA

Cells were seeded into 6-well plates at density of 3×10^4 cells/ml using antibiotic-free DMEM/F12 medium. To silence the expression of AMPKα2, cells were transfected with 45 pmoles of control siRNA or AMPKα2 siRNA using SignalSience AMPKα2 siRNA II (Cell Signaling Technology, Danvers, MA, USA) according to the manufacturer's instruction. They were then further incubated for 5 days with medium exchange once at day 3.

2.12. Statistical analysis

GraphPad Prism 5.03 (GraphPad Software, Inc.) was used for all statistical analyses. One-way analysis of variance (ANOVA) was used for multiple comparisons. Statistical significance was set at $p < 0.05$, $p < 0.01$, and $p < 0.001$.

3. Results

3.1. (R)-crizotinib induces morphology changes of cancer cells

Crizotinib has a chiral carbon. Thus, it has two enantiomers: (*R*)- and (*S*)-crizotinib. To determine ranges of concentrations of crizotinib enantiomers for treating cancer cells and CSC-like cells, SRB assays were conducted (Fig. 1 and Fig. S1). Since growth-inhibiting effects of (*S*)-crizotinib on these cells were not strong at concentration of ~10 μM, its GI_{50} (growth inhibition of 50%) values could not be obtained. GI_{50} values of (*R*)-crizotinib for EML4-ALK positive H3122 and H2228 human non-small lung cancer cells known to be sensitive to crizotinib have been reported to be 62 nM and 121 nM, respectively (Zhang et al., 2011). However, GI_{50} values of (*R*)-crizotinib for NCI-H23, NCI-H460, HCT-15, DLD-1, PC-3, LNCaP, and CSC-like cells were 1.076 ± 0.1607 μM, 2.367 ± 0.2178 μM, 2.938 ± 0.1862 μM, 3.221 ± 0.2718, 2.861 ± 0.2216 μM, 2.937 ± 0.1737 and 5.758 ± 0.6166 μM, respectively. Based on these results, the following *in vitro* assays were conducted using crizotinib at concentrations between 1 and 10 μM.

Morphological changes in cancer cells induced by anticancer agents are often accompanied by alterations to cellular function (Brandhagen

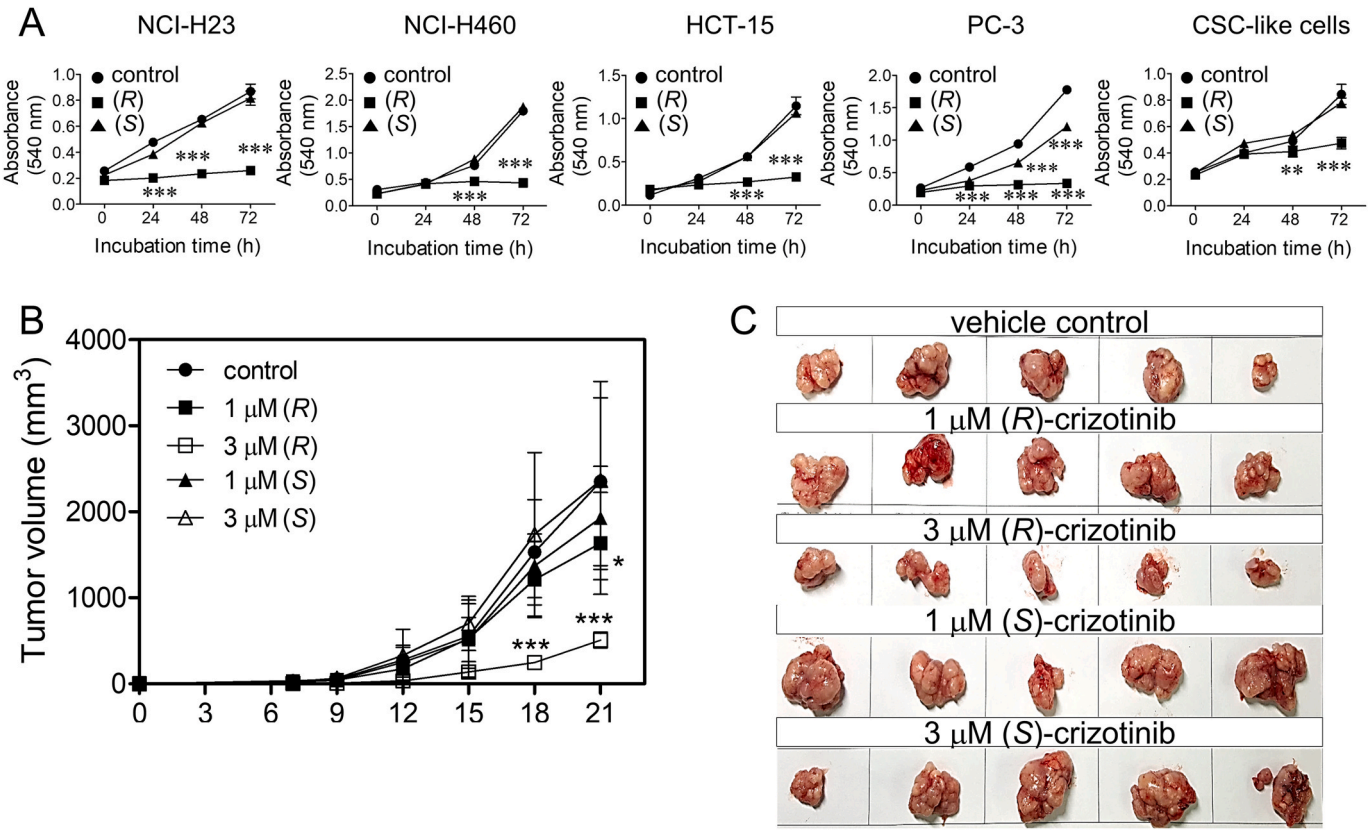

Fig. 4. Pretreatment of cancer and CSC-like cells with (*R*)-crizotinib suppresses their ability to grow *in vitro* and their ability to form tumors *in vivo*. (A) NCI-H23, NCI-H460, HCT-15, PC-3, and PC-3 derived CSC-like cells were incubated with or without 3 μM of (*R*)- or (*S*)-crizotinib for three days. Cells were further incubated in the absence of crizotinib enantiomers for two more days. They were then trypsinized, seeded into a 96-well plate at a density of 2×10^4 cells/ml, allowed to grow, and subjected to sulforhodamine B assay at indicated time points. Data are presented as mean ± SD. **, $p < 0.01$; ***, $p < 0.001$. (B) NCI-H460 cells were incubated with or without crizotinib stereoisomers for 24 h, harvested, and then transplanted to nude mice according to the protocol described in Materials and methods. The growth of tumor was measured at indicated time points. Results are shown as a line graph. (*R*), (*R*)-crizotinib; (*S*), (*S*)-crizotinib. Data are presented as mean ± SD. *, $p < 0.05$; ***, $p < 0.001$. (C) Tumors were collected at the end of the experiment.

et al., 2013; Suzuki et al., 1998; Wang et al., 2016). Fig. 2A shows morphologies of NCI-H23, NCI-H460, HCT-15, PC-3, and CSC-like cells incubated with or without 3 μM of crizotinib enantiomers for 7 days (see Fig. S3 for DLD-1 and LNCaP morphology changes). (*S*)-Crizotinib appeared to induce slight changes in morphologies of these cells. However, obvious changes in morphologies were observed for these cells after treatment with (*R*)-crizotinib. All types of cells treated with (*R*)-crizotinib showed more flattened, enlarged, and spread shapes. To examine if the selectivity of (*R*)- and (S)-crizotinib on phosphorylation of ALK inhibition was maintained at a concentration of 3 μM, cells harvested at 1.5 h after treatment with a crizotinib enantiomer were subjected to western blotting analysis. As shown in Fig. 2B and C, the phosphorylation of ALK was strongly inhibited by 3 μM (*R*)-crizotinib, but not by (*S*)-crizotinib at the same concentration. To examine if the effects of 3 μM (*R*)-crizotinib was simply due to cell death, flow cytometric analysis using Annexin V/PI double staining was performed. No significant change in early apoptotic and late apoptotic/secondary necrotic cell death was observed in all examined cell types (Fig. S2).

3.2. (R)-crizotinib increases sizes of cancer and CSC-like cells

To see if the enlarged and spread shape of cells seen in Fig. 2A and Fig. S3 was accompanied by an increase in the volume of cells, single cell suspensions were prepared after cells were incubated with or without crizotinib enantiomers for 72 h. These cells were then observed under an inverted microscope and photographed (Fig. 3A and S4A). Sizes of these cells increased with increasing concentrations of (*R*)-crizotinib (Fig. 3B and S4B).

3.3. Pretreatment of cancer and CSC-like cells with (R)-crizotinib suppresses their ability to grow in vitro and in vivo

To see if morphological changes of cells observed in Figs. 2 and S3 affect the growth of the cells, NCI-H23, NCI-H460, HCT-15, PC-3, and CSC-like cells were treated with 3 μM of (*R*)- or (*S*)-crizotinib for three days and then allowed to grow in the absence of crizotinib enantiomers for two more days. Cells were then trypsinized and equal numbers of cells were seeded into a 96-well plate. Growths of these cells were then observed (Fig. 4A). Growth of PC-3 cells pretreated with (*S*)-crizotinib was slightly slowed, whereas growths of the other four types of cells were not affected by pretreatment with (*S*)-crizotinib. However, growths of all five types of cells pretreated with (*R*)-crizotinib were very strongly inhibited, suggesting that pretreatment with (*R*)-crizotinib caused most cells to lose their ability to proliferate. Fig. S5 shows that the morphological changes induced by pretreatment with 3 μM (*R*)-crizotinib are not reversible.

To see if cancer cells pretreated with (*R*)-crizotinib might also lose their capability to form tumors *in vivo*, NCI-H460 cells were incubated with or without (*R*)- or (*S*)-crizotinib at 1 μM or 3 μM for 24 h and then transplanted into flanks of Balb/c nude mice (Fig. 4B and C). While pretreatment of NCI-H460 cells with (*S*)-crizotinib did not suppress tumor formation, pretreatment of these cells with (*R*)-crizotinib concentration-dependently inhibited tumor formation, suggesting that pretreatment with (*R*)-crizotinib could alter the ability of NCI-H460 cells to form tumors *in vivo*.

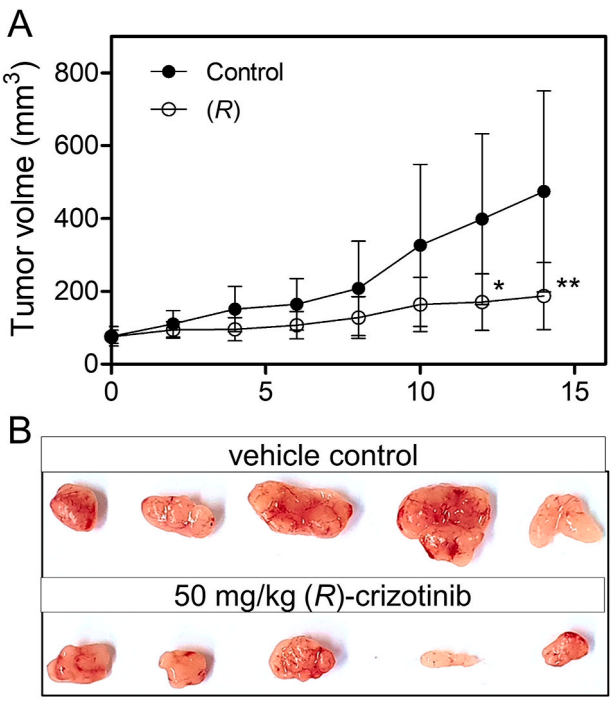

Fig. 5. (*R*)-crizotinib inhibits growth of tumors formed from CSC-like cells. (A) PC-3 derived CSC-like cells were transplanted subcutaneously into nude mice according to the protocol described in Materials and methods. When average volumes of tumors reached about 75 mm^3, (*R*)- or (*S*)-crizotinib was administered intraperitoneally at a dose of 40 mg/kg once a day. (*R*), (*R*)-crizotinib. Data are presented as mean ± SD. *, $p < 0.05$; ***, $p < 0.001$. (B) Tumors were collected at the end of the experiment. In case of (*S*)-crizotinib administration group, the experiment was stopped after 6 doses due to severe weight loss (>15%).

3.4. (*R*)-crizotinib inhibits growths of tumors formed by PC-3 derived CSC-like cells

To determine if growths of tumors formed by CSC-like cells could be inhibited by (*R*)-crizotinib, PC-3 derived CSC-like cells were transplanted subcutaneously in Balb/c nude mice (Fig. 5). When average volumes of tumors reached at about 75 mm^3, 40 mg/kg of (*R*)- or (*S*)-crizotinib was administered intraperitoneally to mice for 2 weeks. However, the experiment for (*S*)-crizotinib was stopped due to severe body weight decrease (greater than 15%). At day 14, (*R*)-crizotinib showed an inhibition of tumor growth of approximately 72% compared to the control.

3.5. (*R*)-crizotinib increases ROS production in four types of cancer cells, but not in CSC-like cells

Previous studies suggest that ROS production is associated with changes in cellular morphology (Alexandrova et al., 2006; Chang et al., 2017). To examine if ROS was involved in the induction of morphological changes in cancer and CSC-like cells, levels of ROS produced by cancer and CSC-like cells treated with (*R*)- or (*S*)-crizotinib were measured (Fig. 6). While (*R*)-crizotinib increased the production of ROS in NCI-H23, NCI-H460, HCT-15, and PC-3 cells in a concentration-dependent manner, it did not increase the production of ROS in CSC-like cells. (*R*)-crizotinib at 10 μM rather decreased the production of ROS in CSC-like cells. These results indicate that ROS is not a common denominator involved in the induction of morphology changes of cancer and CSC-like cells by (*R*)-crizotinib. (*S*)-crizotinib did not cause clear changes in the production of ROS in all five types of cells except PC-3 cells treated with 10 μM.

3.6. (*R*)-crizotinib induces changes in the expression of characteristic marker proteins of cancer and CSC-like cells

NCI-H23 and HCT-15 express CD44; NCI-H460 expresses ALDH1; PC-3 expresses nanog; and CSC-like cells express Oct-4A as characteristic protein markers (Ju et al., 2014; Lee et al., 2019; Leung et al., 2010; Srinual et al., 2017). The expression of CD44, ALDH1, nanog and Oct-4A highly decreased in NCI-H23, NCI-H460, PC-3, and CSC-like cells treated with 3 μM (*R*)-crizotinib for 5 days, respectively, while the expression of CD44 greatly increased in HCT-15 (Fig. 7).

In addition, among many other candidate marker molecules tested, Snail (SNAI1), Slug (SNAI2), and E-cadherin provided meaningful results (Fig. S6). Incubation with 3 μM (*R*)-crizotinib greatly increased the expression of Snail but decreased the expression of Slug in NCI-H23,

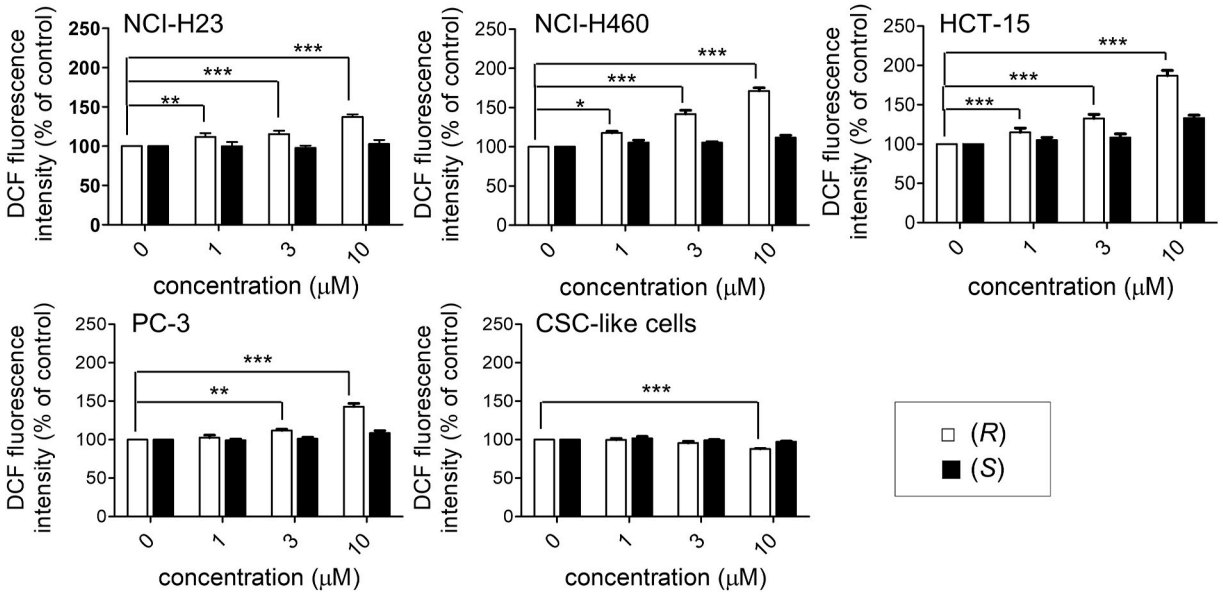

Fig. 6. Crizotinib increases production of ROS in cancer cells, but not in CSC-like cells. NCI-H23, NCI-H460, HCT-15, PC-3, and PC-3 derived CSC-like cells were incubated with (*R*)- or (*S*)-crizotinib at 0, 1, 3, or 10 μM for 48 h and then subjected to ROS assay (n = 4) as described in Materials and methods. White bar, (*R*)-crizotinib; Black bar, (*S*)-crizotinib. Data are presented as mean ± SD. *, $p < 0.05$; ***, $p < 0.001$.

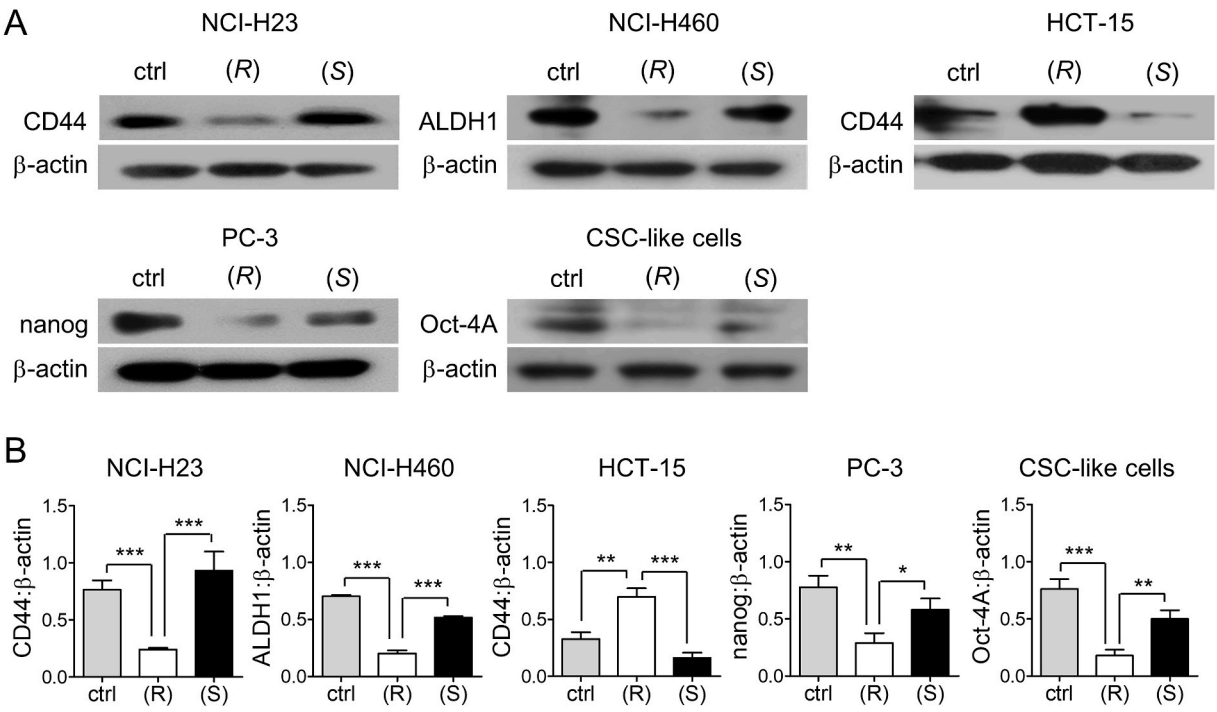

Fig. 7. (*R*)-crizotinib induces changes in the expression of characteristic protein markers of cancer and CSC-like cells. (A) NCI-H23, NCI-H460, HCT-15, PC-3, and PC-3 derived CSC-like cells were incubated with or without 3 μM of (*R*)- or (*S*)-crizotinib for 5 days, harvested, and subjected to western blotting analysis for CD44, ALDH1, nanog, and Oct-4A. (B) Results of band densitometry analysis (n = 3) are shown as bar graphs. Data are presented as mean ± SD. *, $p < 0.05$; **, $p < 0.01$; ***, $p < 0.001$. ctrl: control; (*R*): (*R*)-crizotinib; (*S*): (*S*)-crizotinib.

NCI-H460, HCT-15, DLD-1, PC-3, LNCaP, and PC-3 derived CSC-like cells. Expression levels of E-cadherin were decreased in NCI-H23, NCI-H460, HCT-15, PC-3 and LNCaP cells, but increased in DLD-1 and PC-3 derived CSC-like cells. On the other hand, expression levels of Snail, Slug, and E-cadherin were less affected by treatment with (*S*)-crizotinib. These results demonstrated that the expression of Snail was increased while that of Slug was decreased in the process of morphology changes induced by (*R*)-crizotinib. However, these changes in the expression of Snail and Slug were not correlated with changes in the expression of E-cadherin after treatment with (*R*)-crizotinib.

3.7. (R)-crizotinib inhibits phosphorylation of AMPK, Akt, and SAPK/JNK better than (S)-crizotinib

Since results obtained so far showed that changes in the morphology and properties of cancer and CSC-like cells appeared to be induced mainly by (*R*)-crizotinib rather than by (*S*)-crizotinib, it was necessary to find signal transduction molecules involved in the process of morphology of these cells. Western blot analysis was conducted to see if there were any differences in phosphorylation of signal transduction molecules such as AMPK, Akt, c-Met, SAPK/JNK, ERK1/2, FAK, mTOR, and STAT3 in cancer and CSC-like cells treated with 3 μM of (*R*)- or (*S*)-crizotinib for 1.5 h (Figs. 8 and S8). Phosphorylation levels of ERK1/2 (Fig. 8), FAK (Fig. S8), and mTOR (Fig. S8) were not changed by (*R*)-crizotinib or (*S*)-crizotinib. Thus, ERK1/2, FAK, mTOR, and STAT3 were not key signal transduction molecules involved in the differentiation induced by (*R*)-crizotinib. Phosphorylation levels of c-Met (Fig. 8) and STAT3 (Fig. S8) in cancer cells such as NCI-H23, NCI-H23, HCT-15, and PC-3 cells were decreased more after treatment with (*R*)-crizotinib than those after treatment with (*S*)-crizotinib. However, c-Met and STAT3 were not candidate signaling molecules because their phosphorylation levels in CSC-like cells decreased by (*R*)-crizotinib were almost equal to those by (*S*)-crizotinib. In contrast with these results, phosphorylation levels of AMPK, Akt, and SAPK/JNK were decreased more strongly by (*R*)-crizotinib than by (*S*)-crizotinib, suggesting that inhibition of phosphorylation of AMPK, Akt, and SAPK/JNK might mediate the changes in the morphology and properties of these cells.

3.8. Inhibition of AMPK induces obvious changes in morphologies of cancer and CSC-like cells

Since phosphorylation levels of AMPK, Akt, and SAPK/JNK were more strongly inhibited by (*R*)-crizotinib than by (*S*)-crizotinib (Fig. 8), we next examined whether inhibitors of these signal transduction molecules could mimic the effect of (*R*)-crizotinib on morphology changes. BML-275, BML-257, or SP600125 as an inhibitor of AMPK, Akt, or SAPK/JNK phosphorylation, respectively, was used to treat NCI-H23, NCI-H460, HCT-15, PC-3, and PC-3 derived CSC-like cells for 7 days. Morphologies of these cells were then observed (Fig. 9A). The inhibitor of c-Met (SU11274), whose phosphorylation was not inhibited differentially by enantiomers of crizotinib in CSC-like cells, was also included in this experiment for comparison. Among these inhibitors, BML-275 induced dramatic changes in cell morphologies. All five types of cells treated with 3 μM BML-275 were changed to show flattened, enlarged, and spread shapes, similar to those observed after treatment with 3 μM (*R*)-crizotinib. However, BML-257, SP600125, and SU11274 failed to induce clear changes of these cells.

To further confirm that inhibition of AMPK can induce cell morphology changes, NCI-H23, NCI-H460, HCT-15, PC-3, and PC-3 derived CSC-like cells were transfected with AMPKα2 siRNA for the purpose of silencing the expression of AMPK α2. As is shown in Fig. 9B, morphologies of these cells transfected with AMPKα2 siRNA were greatly changed. These results suggest that inhibition of AMPK activation might be a main regulator involved in morphology changes induced by (*R*)-crizotinib.

3.9. Phosphorylation of acetyl CoA carboxylase is inhibited by (R)-crizotinib in all five types of cells

To find a downstream effector molecule affected by inhibition of

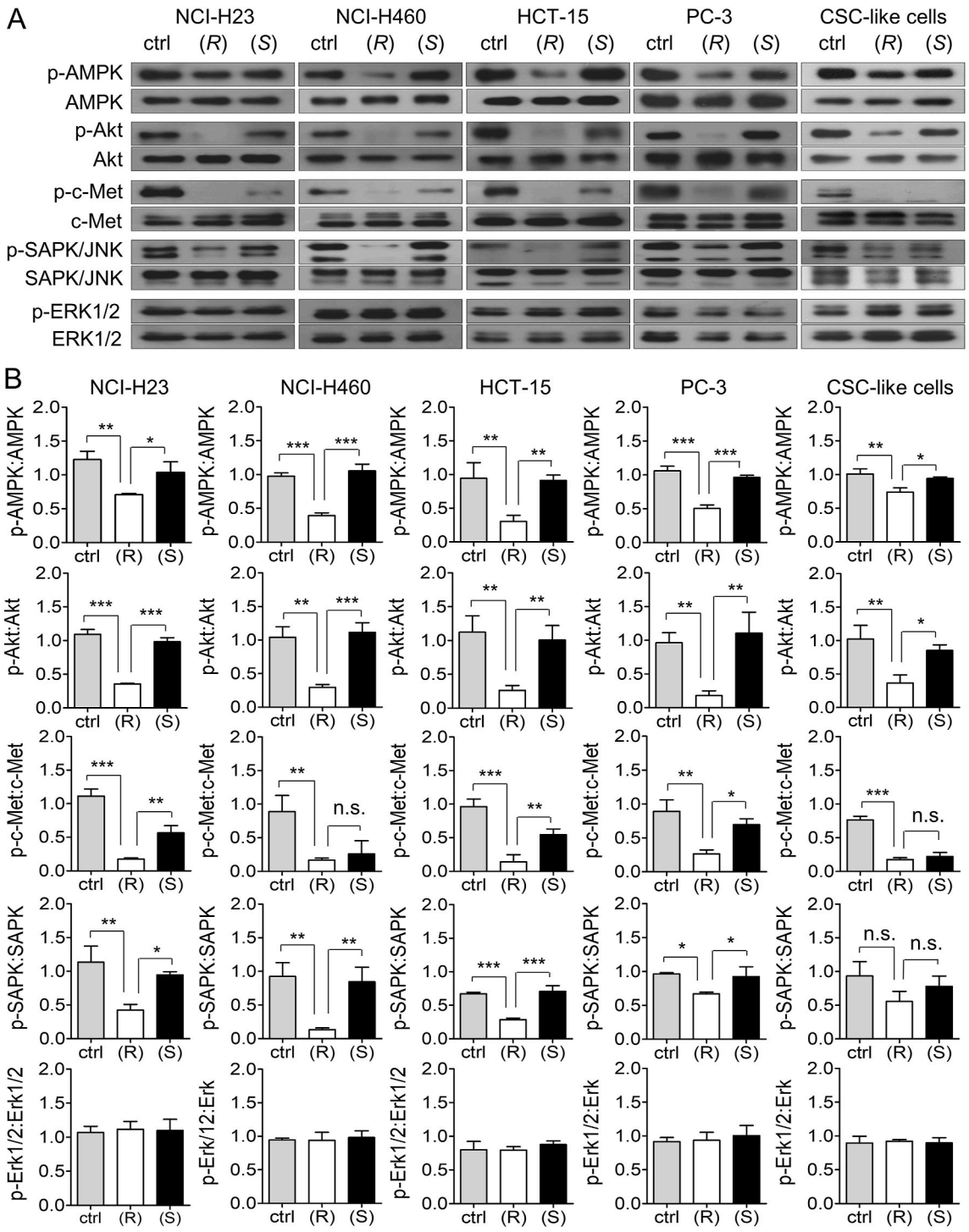

Fig. 8. (*R*)-Crizotinib selectively inhibits phosphorylation of AMPK, Akt, and SAPK/JNK. (A–B) NCI-H23, NCI-H460, HCT-15, PC-3, and PC-3 derived CSC-like cells were incubated with or without 3 μM of (*R*)- or (*S*)-crizotinib for 1.5 h, harvested, and subjected to western blotting analysis. Results of band densitometry analysis (n = 3) are shown as bar graphs. Data are presented as mean ± SD. *, $p < 0.05$; **, $p < 0.01$; ***, $p < 0.001$. ctrl: control; (*R*): (*R*)-crizotinib; (*S*): (*S*)-crizotinib.

AMPK phosphorylation by (*R*)-crizotinib, some signal transduction molecules known as downstream effector molecules, such as acetyl CoA carboxylase (ACC), p21 and p27, were selected to see if (*R*)-crizotinib might lead to any changes in their expression or phosphorylation. The effect of (*R*)-crizotinib on the expression of CDK inhibitors p21 and p27 was variable in five types of cell lines examined. However, levels of phosphorylated ACC (pACC) were significantly decreased by (*R*)-crizotinib in all five types of cell lines examined (Fig. 10), suggesting that suppression of ACC phosphorylation might be a signal transduction event that mediates the morphological changes in these cancer cell lines.

4. Discussion

(*R*)-Crizotinib was originally synthesized as a c-Met and ALK dual inhibitor through a structure-based drug design (Cui et al., 2011). It was approved to treat patients with ALK or ROS1 positive NSCLC. However, efforts to expand its use for various types of cancer have been actively undertaken (Ayoub et al., 2021; Khalil et al., 2020). It is believed that

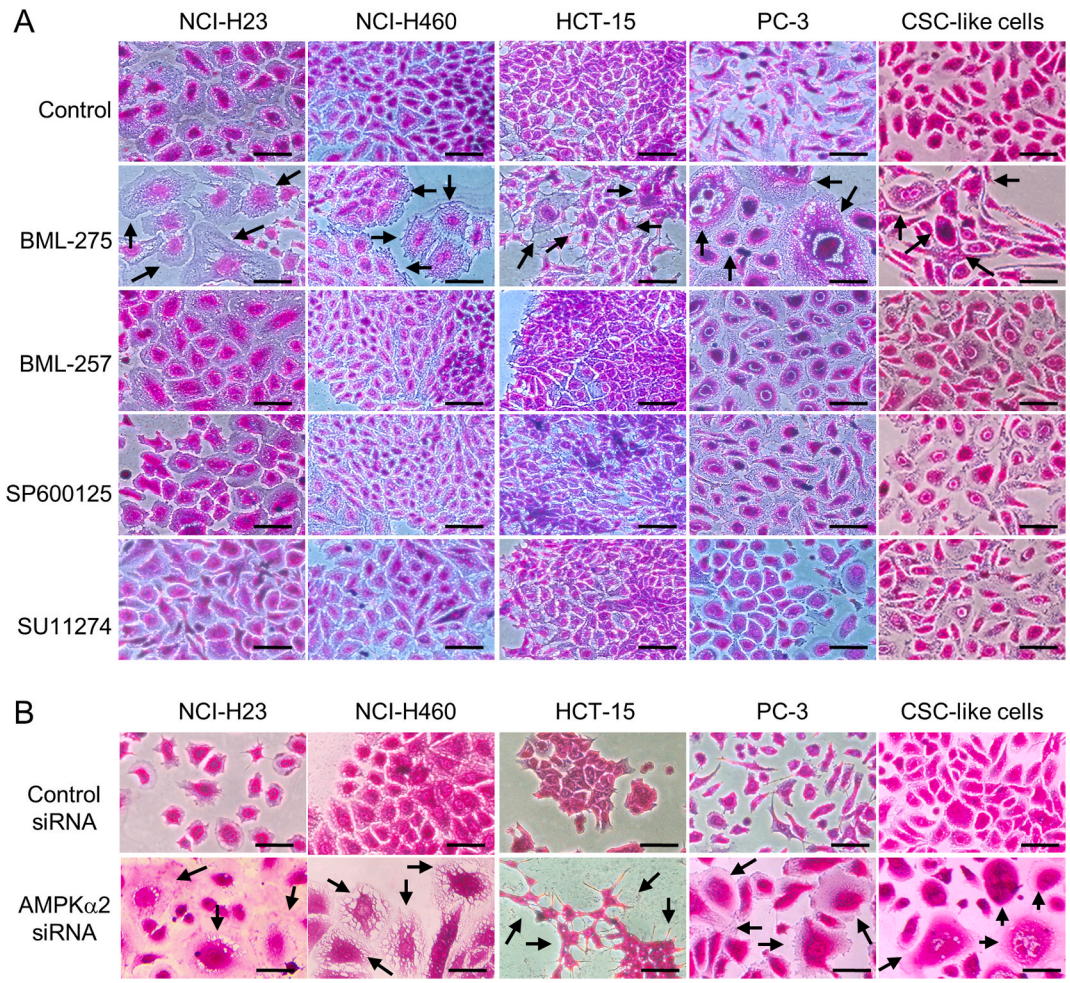

Fig. 9. BML-275 as an AMPK inhibitor and silencing of AMPKα2 expression induce morphology changes of cancer and CSC-like cells. (A) Cells were incubated with or without 3 μM of BML-275, BML-257, SU11274, and SP600125 for 7 days and then stained with 0.4% SRB solution. (B) Cells were transfected with AMPK2α siRNA according to the protocol described in Materials and methods, incubated for 5 days, and then stained with 0.4% SRB solution. Representative images (n = 3) are shown. Black arrows indicate cells whose morphologies are changed. Scale bar: 50 μm.

further studies to identify its mechanisms of action that may not be directly related to ALK or ROS1 will help us understand its anticancer activity in more details. Among various efforts for discovering its new mode of action, ICD induced by a high concentration (~10 μM) of crizotinib is a good example (Liu et al., 2019a, 2019b).

Differentiation therapy for cancer has long been proposed as an attempt to induce differentiation such that CSCs lose their key properties. (de The, 2018). The purpose of the present study, which is similar to that of differentiation therapy, was to observe and investigate whether either crizotinib enantiomer induces the loss of key properties of cancer and CSC-like cells. Interestingly, when two NSCLC cell lines (NCI-H23 and NCI-H460), two colon cancer cell line (HCT-15, DLD-1), two prostate cancer cell line (PC-3, LNCaP), and one PC-3 derived CSC-like cell line were treated with each enantiomer at 3 μM, a concentration that was much higher than GI_{50} values (62–121 nM) of (*R*)-crizitinib against EML4-ALK-positive H3122 and H2228 human non-small lung cancer cells, only (*R*)-crizotinib greatly induced morphology and size changes for all seven types of cells examined. As mentioned in the results section, the effects of (*R*)-crizotinib on cellular morphology raise the possibility of altering the functions and characteristics of cancer cells.

The phosphorylation of ALK was strongly inhibited by a high concentration (3 μM) of (*R*)-crizotinib, but not by (*S*)-crizotinib at the same concentration (Fig. 2B and C). These results indicate that ALK is expressed in all cancer cells examined and that the pattern of ALK inhibition by (*R*)- or (*S*)-crizotinib at a high concentration can also be maintained. Contrary to our results, previous studies have reported that NCI-H23 cells are ALK negative (Noh et al., 2018; Zhang et al., 2011). Such discrepancy might be due to difference in experimental design between laboratories. In fact, a recent report has shown that ALK is expressed at a low level in NCI-H23 cells (Koh et al., 2016).

In addition to cell morphology change, changes in cell size (Figs. 3 and S4) further strengthen the possibility that these phenotypical changes might accompany permanent changes in the expression or structures of cellular components. As shown in Figs. 4A and S5, the proliferation of cells pretreated with 3 μM (*R*)-crizotinib almost stopped, and the morphological changes were maintained even in the absence of (*R*)-crizotinib, further supporting the idea of permanent change of the intracellular environment of these cells. Results of nude mouse xenograft experiments suggest that (*R*)-crizotinib could suppress CSC cells as well as normal cancer cells *in vivo* (Fig. 4B and C, and 5). In Fig. 5, (*R*)- and (*S*)-crizotinib were administered at the same dose of 40 mg/kg for comparison. However, the experiment for (*S*)-crizotinib had to be stopped due to severe body weight loss. It appeared that the toxicity of (*S*)-crizotinib was greater than that of (*R*)-crizotinib. Previous studies have used a dose of (*S*)-crizotinib at 10 or 15 mg/kg and 50 mg/kg of (*R*)-crizotinib for *in vivo* tumor xenograft (Dai et al., 2017; Fang et al., 2014; Ji et al., 2018). The reason that low doses of (*S*)-crizotinib were used in their studies might be because high doses of (*S*)-crizotinib were toxic to nude mice.

The loss of cancer cell properties is expected to be accompanied by

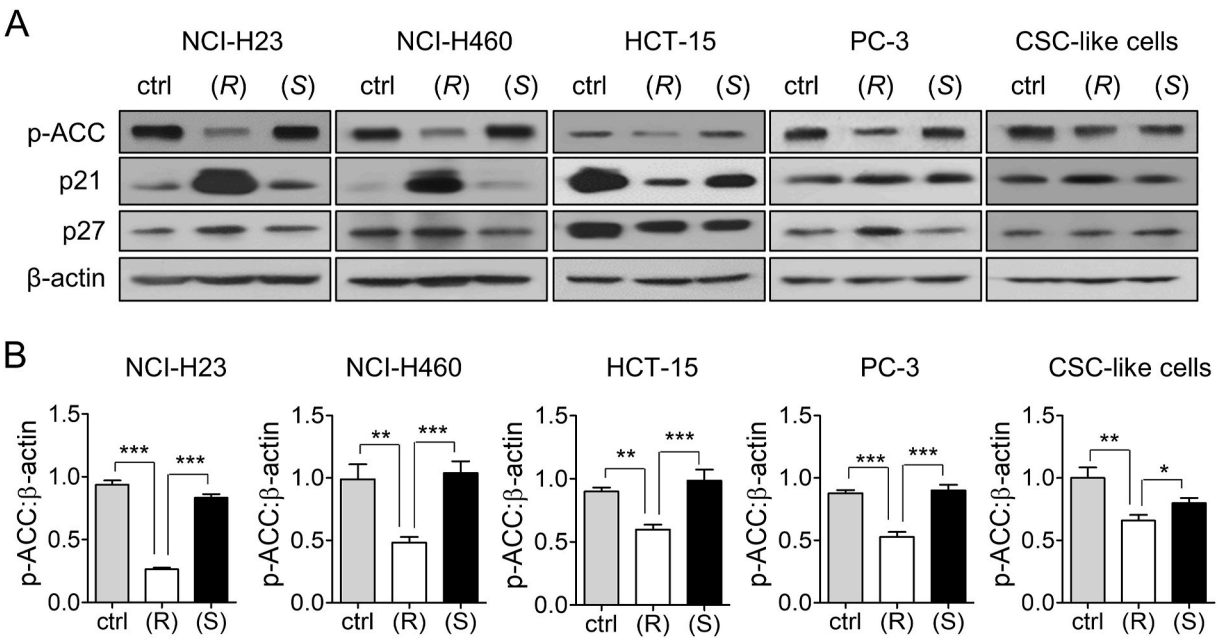

Fig. 10. Phosphorylation of acetyl CoA carboxylase is inhibited by (*R*)-crizotinib. (A) Cells were incubated with 3 μM of (*R*)- or (*S*)-crizotinib for 24 h and then subjected to western blotting analysis as described in Materials and methods. (B) Results of band densitometry analysis (p-ACC:β-actin) (n = 3) are shown as bar graphs. ctrl: control, (R): (*R*)-crizotinib; (S): (*S*)-crizotinib. Data are presented as mean ± SD. *, $p < 0.05$; ***, $p < 0.001$.

changes in the expression patterns of characteristic proteins. To determine whether the alterations in morphology and size of cancer and CSC-like cells induced the loss of cancer cell properties, changes in the expression of characteristic protein markers, such as CD44, ALDH1, nanog, and Oct-4A, in cancer and CSC-like cells were examined. As shown in Fig. 7, significant changes in the expression levels of these markers were induced by 3 μM (*R*)-crizotinib, suggesting that the properties of these cells were altered. Significant changes were also observed in the expression levels of E-cadherin, Snail, and Slug in the cells treated with 3 μM (*R*)-crizotinib (Fig. S6). E-cadherin expression is often, although not always, reduced during epithelial-mesenchymal transition (EMT) (Canel et al., 2013). Snail and Slug are transcription factors known to promote EMT and suppress the expression of E-cadherin (Wang et al., 2013). Interestingly, expression levels of Snail were increased in all cell types examined whereas those of slug were decreased. Expression levels of E-cadherin were decreased in some types of cells (NCI-H23, NCI-H460, HCT-15, and PC-3), but increased in other types of cells (DLD-1 and PC-3 derived CSC-like cells). The expression pattern of E-cadherin was not correlated with that of Snail or Slug. Since E-cadherin is linked to cytoskeletons such as actin fibers and microtubules (Brieher and Yap, 2013), its increased or decreased expression might be related to changes of morphology or behavior of cells (Al Moustafa et al., 1999; Chen et al., 2014; Molina-Ortiz et al., 2009; Padmanaban et al., 2019). Morphology changes and migration inhibition (Fig. S7) of cancer and CSC-like cells induced by (*R*)-crizotinib occurred regardless of increase or decrease of E-cadherin expression, suggesting that E-cadherin did not participate as a key player in the process of differentiation induction by (*R*)-crizotinib.

A possible mechanism underlying the morphological changes in the cancer and CSC-like cells is ROS, as changes in ROS production have been linked to morphological changes in cells (Alexandrova et al., 2006; Chang et al., 2017). (*R*)-crizotinib concentration-dependently increased the production of ROS in NCI-H23, NCI-H460, HCT-15 and PC-3 cells. However, ROS production in PC-3 derived CSC-like cells was not increased by any enantiomer of crizotinib. This might be due to the presence of machinery such as CD44 and xCT that confer ROS defense in CSC-like cells (Ishimoto et al., 2011). These results suggested that ROS was not a common factor that induced the changes in morphology and size of cells used in the present study.

The phosphorylation of AMPK, Akt, and SAPK/JNK among signal transducing molecules examined was selectively inhibited by (*R*)-crizotinib in all five types of cells (Fig. 8). The phosphorylation of c-Met was inhibited to a similar extent by both crizotinib enantiomers in all types of cells examined and SU11274, a c-Met inhibitor, did not induce morphology changes in any type of cells. Thus, c-Met was not a key cellular factor that played a major role in the (*R*)-crizotinib-induced changes in morphology and properties in these cells.

Our results (Fig. 9) showed that an AMPK inhibitor and AMPKα2 siRNA induced morphology changes in cells, suggesting that inhibition of AMPK might have mediated the activity of (*R*)-crizotinib in inducing changes in morphology and properties of the cells used in this study. A report that AMPK knockdown altered the morphology and function of placental trophoblast cells (Carey et al., 2014) corroborates with our results, where AMPK inhibition induced morphological changes in cancer and CSC-like cells. AMPK can modulate many kinds of downstream regulators (Garcia and Shaw, 2017). CDK inhibitors p21 and p27 are reported to be involved in morphological changes of cancer cells (Chen et al., 1999; Dirks et al., 1997). However, they were excluded from candidates of downstream effector molecules of AMPK because the expression of these two molecules was suppressed or enhanced irregularly between cancer cell lines (Fig. 10). ACC is a fatty acid metabolism key regulator and a downstream effector molecule of AMPK. ACC is associated with metastatic potential of breast cancer cells. ACC suppresses breast cancer migration and invasion, which affect metastatic potential of breast cancer cells and acute myeloid leukemia development (Ito et al., 2021; Rios Garcia et al., 2017). Although further study is needed, results of these previous studies and our study suggest that inhibition of ACC phosphorylation might be one of downstream pathways that mediate signals for inducing changes in morphology and properties of cancer cells.

In conclusion, results of the present study suggest that (*R*)-crizotinib might have off-target effects such as changing the morphology and properties of cancer cells at high concentrations. Further studies are needed to elucidate the exact relations of AMPK with downstream effectors in the process of altering cancer cell properties and morphology. The present discovery of the involvement of AMPK inhibition in the loss

of malignant properties of cancer and CSC-like cells induced by (*R*)-crizotinib is expected to widen ways for using crizotinib in the treatment of patients suffering from various types of cancer.

Funding

This research was supported by grants [NRF-2014R1A1A2059237 and NRF-2019R1F1A1061276 (SKP), and NRF-2019R1A6A1A03031807 (YB)] of the National Research Foundation (NRF) of Korea.

Compliance with ethics guidelines

Animal studies were conducted according to procedures approved by Institutional Animal Care & Use Committee (IACUC) of Korea University, Seoul, Korea.

Data availability

Data will be made available upon reasonable request.

CRediT authorship contribution statement

Tae Hyun Kim: Investigation, Formal analysis, Data curation, Writing – review & editing. **Jong Hyeok Park:** Investigation, Formal analysis, Data curation, Writing – review & editing. **Jooyeon Park:** Investigation, Formal analysis, Data curation, Writing – review & editing. **Dong Min Son:** Investigation, Formal analysis. **Ji-Young Baek:** Investigation, Formal analysis. **Hee Jun Jang:** Investigation, Formal analysis, Data curation. **Won Ki Jung:** Investigation, Formal analysis, Data curation. **Youngjoo Byun:** Conceptualization, Funding acquisition. **Sang Kyum Kim:** Conceptualization, Methodology, Writing – review & editing. **Song-Kyu Park:** Conceptualization, Methodology, Formal analysis, Writing – original draft, Writing – review & editing, Supervision, Funding acquisition.

Declaration of competing interest

The authors declare that they have no known competing financial interests or personal relationships that could have appeared to influence the work reported in this paper.

Appendix A. Supplementary data

Supplementary data to this article can be found online at https://doi.org/10.1016/j.ejphar.2021.174525.

References

Al Moustafa, A.E., Yansouni, C., Alaoui-Jamali, M.A., O'Connor-McCourt, M., 1999. Up-regulation of E-cadherin by an anti-epidermal growth factor receptor monoclonal antibody in lung cancer cell lines. Clin. Canc. Res. 5, 681–686.

Alexandrova, A.Y., Kopnin, P.B., Vasiliev, J.M., Kopnin, B.P., 2006. ROS up-regulation mediates Ras-induced changes of cell morphology and motility. Exp. Cell Res. 312, 2066–2073.

Ayoub, N.M., Ibrahim, D.R., Alkhalifa, A.E., Al-Husein, B.A., 2021. Crizotinib induced antitumor activity and synergized with chemotherapy and hormonal drugs in breast cancer cells via downregulating MET and estrogen receptor levels. Invest. N. Drugs 39, 77–88.

Bergethon, K., Shaw, A.T., Ou, S.H., Katayama, R., Lovly, C.M., McDonald, N.T., Massion, P.P., Siwak-Tapp, C., Gonzalez, A., Fang, R., Mark, E.J., Batten, J.M., Chen, H., Wilner, K.D., Kwak, E.L., Clark, J.W., Carbone, D.P., Ji, H., Engelman, J.A., Mino-Kenudson, M., Pao, W., Iafrate, A.J., 2012. ROS1 rearrangements define a unique molecular class of lung cancers. J. Clin. Oncol. 30, 863–870.

Brandhagen, B.N., Tieszen, C.R., Ulmer, T.M., Tracy, M.S., Goyeneche, A.A., Telleria, C. M., 2013. Cytostasis and morphological changes induced by mifepristone in human metastatic cancer cells involve cytoskeletal filamentous actin reorganization and impairment of cell adhesion dynamics. BMC Canc. 13, 35.

Brieher, W.M., Yap, A.S., 2013. Cadherin junctions and their cytoskeleton(s). Curr. Opin. Cell Biol. 25, 39–46.

Canel, M., Serrels, A., Frame, M.C., Brunton, V.G., 2013. E-cadherin-integrin crosstalk in cancer invasion and metastasis. J. Cell Sci. 126, 393–401.

Carey, E.A., Albers, R.E., Doliboa, S.R., Hughes, M., Wyatt, C.N., Natale, D.R., Brown, T. L., 2014. AMPK knockdown in placental trophoblast cells results in altered morphology and function. Stem Cell. Dev. 23, 2921–2930.

Chang, Y.T., Huang, C.Y., Tang, J.Y., Liaw, C.C., Li, R.N., Liu, J.R., Sheu, J.H., Chang, H. W., 2017. Reactive oxygen species mediate soft corals-derived sinuleptolide-induced antiproliferation and DNA damage in oral cancer cells. OncoTargets Ther. 10, 3289–3297.

Chen, A., Beetham, H., Black, M.A., Priya, R., Telford, B.J., Guest, J., Wiggins, G.A., Godwin, T.D., Yap, A.S., Guilford, P.J., 2014. E-cadherin loss alters cytoskeletal organization and adhesion in non-malignant breast cells but is insufficient to induce an epithelial-mesenchymal transition. BMC Canc. 14, 552.

Chen, Y.J., Lin, J.K., Lin-Shiau, S.Y., 1999. Proliferation arrest and induction of CDK inhibitors p21 and p27 by depleting the calcium store in cultured C6 glioma cells. Eur. J. Cell Biol. 78, 824–831.

Christensen, J.G., Zou, H.Y., Arango, M.E., Li, Q., Lee, J.H., McDonnell, S.R., Yamazaki, S., Alton, G.R., Mroczkowski, B., Los, G., 2007. Cytoreductive antitumor activity of PF-2341066, a novel inhibitor of anaplastic lymphoma kinase and c-Met, in experimental models of anaplastic large-cell lymphoma. Mol. Canc. Therapeut. 6, 3314–3322.

Cui, J.J., Tran-Dube, M., Shen, H., Nambu, M., Kung, P.P., Pairish, M., Jia, L., Meng, J., Funk, L., Botrous, I., McTigue, M., Grodsky, N., Ryan, K., Padrique, E., Alton, G., Timofeevski, S., Yamazaki, S., Li, Q., Zou, H., Christensen, J., Mroczkowski, B., Bender, S., Kania, R.S., Edwards, M.P., 2011. Structure based drug design of crizotinib (PF-02341066), a potent and selective dual inhibitor of mesenchymal-epithelial transition factor (c-MET) kinase and anaplastic lymphoma kinase (ALK). J. Med. Chem. 54, 6342–6363.

Dai, X., Guo, G., Zou, P., Cui, R., Chen, W., Chen, X., Yin, C., He, W., Vinothkumar, R., Yang, F., Zhang, X., Liang, G., 2017. (S)-crizotinib induces apoptosis in human non-small cell lung cancer cells by activating ROS independent of MTH1. J. Exp. Clin. Cancer Res. 36, 120.

de The, H., 2018. Differentiation therapy revisited. Nat. Rev. Canc. 18, 117–127.

Dirks, P.B., Patel, K., Hubbard, S.L., Ackerley, C., Hamel, P.A., Rutka, J.T., 1997. Retinoic acid and the cyclin dependent kinase inhibitors synergistically alter proliferation and morphology of U343 astrocytoma cells. Oncogene 15, 2037–2048.

Enane, F.O., Saunthararajah, Y., Korc, M., 2018. Differentiation therapy and the mechanisms that terminate cancer cell proliferation without harming normal cells. Cell Death Dis. 9, 912.

Fang, D.D., Zhang, B., Gu, Q., Lira, M., Xu, Q., Sun, H., Qian, M., Sheng, W., Ozeck, M., Wang, Z., Zhang, C., Chen, X., Chen, K.X., Li, J., Chen, S.H., Christensen, J., Mao, M., Chan, C.C., 2014. HIP1-ALK, a novel ALK fusion variant that responds to crizotinib. J. Thorac. Oncol. 9, 285–294.

Garcia, D., Shaw, R.J., 2017. AMPK: mechanisms of cellular energy sensing and restoration of metabolic balance. Mol. Cell. 66, 789–800.

Huber, K.V., Salah, E., Radic, B., Gridling, M., Elkins, J.M., Stukalov, A., Jemth, A.S., Gokturk, C., Sanjiv, K., Stromberg, K., Pham, T., Berglund, U.W., Colinge, J., Bennett, K.L., Loizou, J.I., Helleday, T., Knapp, S., Superti-Furga, G., 2014. Stereospecific targeting of MTH1 by (S)-crizotinib as an anticancer strategy. Nature 508, 222–227.

Ishimoto, T., Nagano, O., Yae, T., Tamada, M., Motohara, T., Oshima, H., Oshima, M., Ikeda, T., Asaba, R., Yagi, H., Masuko, T., Shimizu, T., Ishikawa, T., Kai, K., Takahashi, E., Imamura, Y., Baba, Y., Ohmura, M., Suematsu, M., Baba, H., Saya, H., 2011. CD44 variant regulates redox status in cancer cells by stabilizing the xCT subunit of system xc(-) and thereby promotes tumor growth. Canc. Cell 19, 387–400.

Ito, H., Nakamae, I., Kato, J.Y., Yoneda-Kato, N., 2021. Stabilization of fatty acid synthesis enzyme acetyl-CoA carboxylase 1 suppresses acute myeloid leukemia development. J. Clin. Invest. 131.

Ji, J., Chen, W., Lian, W., Chen, R., Yang, J., Zhang, Q., Weng, Q., Khan, Z., Hu, J., Chen, X., Zou, P., Chen, X., Liang, G., 2018. (S)-crizotinib reduces gastric cancer growth through oxidative DNA damage and triggers pro-survival akt signal. Cell Death Dis. 9, 660.

Ju, S.Y., Chiou, S.H., Su, Y., 2014. Maintenance of the stemness in CD44(+) HCT-15 and HCT-116 human colon cancer cells requires miR-203 suppression. Stem Cell Res. 12, 86–100.

Jung, H.S., Lee, S.I., Kang, S.H., Wang, J.S., Yang, E.H., Jeon, B., Myung, J., Baek, J.Y., Park, S.K., 2017. Monoclonal antibodies against autocrine motility factor suppress gastric cancer. Oncol Lett 13, 4925–4932.

Kang, M.R., Park, S.K., Lee, C.W., Cho, I.J., Jo, Y.N., Yang, J.W., Kim, J.A., Yun, J., Lee, K.H., Kwon, H.J., Kim, B.W., Lee, K., Kang, J.S., Kim, H.M., 2012. Widdrol induces apoptosis via activation of AMP-activated protein kinase in colon cancer cells. Oncol. Rep. 27, 1407–1412.

Khalil, S., Ghafoor, T., Raja, A.K.F., 2020. Inflammatory myofibroblastic tumor: a rare presentation and an effective treatment with crizotinib. Case Rep Oncol Med 2020, 6923103.

Koh, J., Jang, J.Y., Keam, B., Kim, S., Kim, M.Y., Go, H., Kim, T.M., Kim, D.W., Kim, C. W., Jeon, Y.K., Chung, D.H., 2016. EML4-ALK enhances programmed cell death-ligand 1 expression in pulmonary adenocarcinoma via hypoxia-inducible factor (HIF)-1alpha and STAT3. OncoImmunology 5, e1108514.

Lee, S.I., Roney, M.S.I., Park, J.H., Baek, J.Y., Park, J., Kim, S.K., Park, S.K., 2019. Dopamine receptor antagonists induce differentiation of PC-3 human prostate cancer cell-derived cancer stem cell-like cells. Prostate 79, 720–731.

Leung, E.L., Fiscus, R.R., Tung, J.W., Tin, V.P., Cheng, L.C., Sihoe, A.D., Fink, L.M., Ma, Y., Wong, M.P., 2010. Non-small cell lung cancer cells expressing CD44 are enriched for stem cell-like properties. PloS One 5, e14062.

Liu, P., Zhao, L., Kepp, O., Kroemer, G., 2019a. Crizotinib - a tyrosine kinase inhibitor that stimulates immunogenic cell death. OncoImmunology 8, 1596652.
Liu, P., Zhao, L., Pol, J., Levesque, S., Petrazzuolo, A., Pfirschke, C., Engblom, C., Rickelt, S., Yamazaki, T., Iribarren, K., Senovilla, L., Bezu, L., Vacchelli, E., Sica, V., Melis, A., Martin, T., Xia, L., Yang, H., Li, Q., Chen, J., Durand, S., Aprahamian, F., Lefevre, D., Broutin, S., Paci, A., Bongers, A., Minard-Colin, V., Tartour, E., Zitvogel, L., Apetoh, L., Ma, Y., Pittet, M.J., Kepp, O., Kroemer, G., 2019b. Crizotinib-induced immunogenic cell death in non-small cell lung cancer. Nat. Commun. 10, 1486.
Molina-Ortiz, I., Bartolome, R.A., Hernandez-Varas, P., Colo, G.P., Teixido, J., 2009. Overexpression of E-cadherin on melanoma cells inhibits chemokine-promoted invasion involving p190RhoGAP/p120ctn-dependent inactivation of RhoA. J. Biol. Chem. 284, 15147–15157.
Noh, K.W., Sohn, I., Song, J.Y., Shin, H.T., Kim, Y.J., Jung, K., Sung, M., Kim, M., An, S., Han, J., Lee, S.H., Lee, M.S., Choi, Y.L., 2018. Integrin beta3 inhibition enhances the antitumor activity of ALK inhibitor in ALK-rearranged NSCLC. Clin. Canc. Res. 24, 4162–4174.
Padmanaban, V., Krol, I., Suhail, Y., Szczerba, B.M., Aceto, N., Bader, J.S., Ewald, A.J., 2019. E-cadherin is required for metastasis in multiple models of breast cancer. Nature 573, 439–444.
Patel, S.P., Pakkala, S., Pennell, N.A., Reckamp, K.L., Lanzalone, S., Polli, A., Tarazi, J., Robert-Vizcarrondo, F., 2020. Phase Ib study of crizotinib plus pembrolizumab in patients with previously untreated advanced non-small cell lung cancer with ALK translocation. Oncol. 25, 562–e1012.
Rios Garcia, M., Steinbauer, B., Srivastava, K., Singhal, M., Mattijssen, F., Maida, A., Christian, S., Hess-Stumpp, H., Augustin, H.G., Muller-Decker, K., Nawroth, P.P., Herzig, S., Berriel Diaz, M., 2017. Acetyl-CoA carboxylase 1-dependent protein acetylation controls breast cancer metastasis and recurrence. Cell Metabol. 26, 842–855 e845.
Skehan, P., Storeng, R., Scudiero, D., Monks, A., McMahon, J., Vistica, D., Warren, J.T., Bokesch, H., Kenney, S., Boyd, M.R., 1990. New colorimetric cytotoxicity assay for anticancer-drug screening. J Natl Canc. Inst 82, 1107–1112.
Srinual, S., Chanvorachote, P., Pongrakhananon, V., 2017. Suppression of cancer stem-like phenotypes in NCI-H460 lung cancer cells by vanillin through an Akt-dependent pathway. Int. J. Oncol. 50, 1341–1351.
Suzuki, N., Del Villar, K., Tamanoi, F., 1998. Farnesyltransferase inhibitors induce dramatic morphological changes of KNRK cells that are blocked by microtubule interfering agents. Proc. Natl. Acad. Sci. U. S. A. 95, 10499–10504.
Tripathi, A., Supko, J.G., Gray, K.P., Melnick, Z.J., Regan, M.M., Taplin, M.E., Choudhury, A.D., Pomerantz, M.M., Bellmunt, J., Yu, C., Sun, Z., Srinivas, S., Kantoff, P.W., Sweeney, C.J., Harshman, L.C., 2020. Dual blockade of c-MET and the androgen receptor in metastatic castration-resistant prostate cancer: a Phase I study of concurrent enzalutamide and crizotinib. Clin. Canc. Res. 26, 6122–6131.
Wang, Y., Shi, J., Chai, K., Ying, X., Zhou, B.P., 2013. The role of Snail in EMT and tumorigenesis. Curr. Cancer Drug Targets 13, 963–972.
Wang, Y., Tian, P., Xia, L., Li, L., Han, R., Zhu, M., Lizaso, A., Qin, T., Li, M., Yu, B., Mao, X., Han-Zhang, H., He, Y., 2020. The clinical efficacy of combinatorial therapy of EGFR-TKI and crizotinib in overcoming MET amplification-mediated resistance from prior EGFR-TKI therapy. Lung Canc. 146, 165–173.
Wang, Y.L., Liui, H.L., Fu, R.G., Wang, Z.W., Ren, H.T., Dai, Z.J., Jing, Y.Y., Li, Y., 2016. HDAC inhibitor oxamflatin induces morphological changes and has strong cytostatic effects in ovarian cancer cell lines. Curr. Mol. Med. 16, 232–242.
Zhang, S., Wang, F., Keats, J., Zhu, X., Ning, Y., Wardwell, S.D., Moran, L., Mohemmad, Q.K., Anjum, R., Wang, Y., Narasimhan, N.I., Dalgarno, D., Shakespeare, W.C., Miret, J.J., Clackson, T., Rivera, V.M., 2011. Crizotinib-resistant mutants of EML4-ALK identified through an accelerated mutagenesis screen. Chem. Biol. Drug Des. 78, 999–1005.